Pramana – J. Phys. (2017) 88: 27
DOI 10.1007/s12043-016-1325-4

Factors controlling phase formation of novel Sr-based Y-type hexagonal ferrite nanoparticles

R THOLKAPPIYAN[1,2,*], K VISHISTA[1] and FATHALLA HAMED[2]

[1]Department of Physics, College of Engineering, Guindy, Anna University, Chennai 600 025, India
[2]Department of Physics, College of Science, United Arab Emirates University, Al Ain, United Arab Emirates
*Corresponding author. E-mail: thols2006@gmail.com

MS received 15 September 2015; revised 31 December 2015; accepted 17 June 2016; published online 4 January 2017

Abstract. New Sr-based Y-type nanocrystalline hexagonal ferrites with a nominal chemical composition of $Sr_2Mg_2Fe_{12}O_{22}$ (Sr_2Y) were prepared by autocombustion from mixtures of $Sr(NO_3)_2$, $Mg(NO_3)_2{\cdot}6H_2O$ and $Fe(NO_3)_3{\cdot}9H_2O$. The newly prepared Sr_2Y nanocrystalline particles were characterized by powder X-ray diffraction (XRD). A well crystalline phase of Sr_2Y with hexagonal crystal structure was observed. Fourier transform infrared spectroscopy (FTIR) studies revealed the information about the positions of the ions and their bonds within the lattice structure of the Sr_2Y. The chemical elements and their oxidation states in the Sr_2Y hexaferrites were determined using X-ray photoelectron spectroscopy (XPS). The XRD, FTIR and XPS studies confirmed the formation of $Sr_2Mg_2Fe_{12}O_{22}$ hexaferrites. The morphology and porosity of the prepared Sr_2Y nanocrystalline Sr_2Y hexaferrite particles were studied by field emission scanning electron microscopy. The magnetic properties of Sr_2Y hexaferrites showed dependence on the methods of preparation conditions and calcination treatments. The values of coercivity, saturation magnetization and retentivity were in the range of 21.33–19.66 kA m^{-1}, 42.44–38.72 emu g^{-1} and 10.05–13.19 emu g^{-1} respectively.

Keywords. Hexagonal ferrites; combustion process; X-ray photoelectron spectroscopy; glycine; oxidation state.

PACS Nos 41.50.+h; 75; 81

1. Introduction

Ferrite-based magnetic materials have continued to attract attention due to their interesting magnetic properties. Recently, hexagonal ferrites have attracted more attention due to their use as permanent magnets [1]. Technological requirements of future applications including electronics devices, transformers and magnetic storage circuits require that material scientists continue to tune in the properties such as microstructure, homogeneity, particle shape and size, because such factors affect the extrinsic required magnetic behavior [2]. Among the various types of hexagonal ferrites, Y-type ferrites have proved to be the most promising candidates in magneto-optic recording devices, high-density recording media, spintronics, magnetic cell separation and microwave absorption devices [3,4]. Sr_2Y comes under Y-type hexaferrite materials with the general formula $A_2Me_2Fe_{12}O_{22}$ where A and Me refer to divalent metal ions distributed among six sublattices (two tetrahedral and four octahedral).

Even though various techniques such as chemical co-precipitation, sol–gel synthesis, hydrothermal method, self-propagating high temperature and mechanical alloying have been adopted in the synthesis of hexagonal ferrites, the autocombustion synthesis is more cost effective where the entire reaction process takes 20 min. The autocombustion method provides a great opportunity for large-scale production of nanoparticles in a short span of time. This makes autocombustion a viable method of production for industrial manufacturing of ceramic materials.

Up to date, no studies were reported on Sr_2Y hexaferrite. In the present work, we shall report the synthesis of Sr_2Y hexaferrite by autocombustion using glycine as the fuel. The mechanism for the phase formation of Sr_2Y nanoparticles will be clearly presented and discussed. We have been able to produce an almost

pure single phase of Sr_2Y hexaferrites. The newly prepared nanocrystalline Sr_2Y hexaferrite particles were characterized by powder X-ray diffraction (XRD) and Fourier transform infrared spectroscopy (FTIR) to confirm the position of ions within the prepared Sr_2Y hexaferrites. The chemical elements and the oxidation states in the prepared nanocrystalline Sr_2Y hexaferrites were examined by X-ray photoelectron spectroscopy (XPS). The surface morphology was analysed by field emission scanning electron microscope (FESEM). The magnetic properties of the prepared Sr_2Y samples were measured by vibrating sample magnetometer (VSM). The preparation of the novel Sr_2Y hexaferrite nanocrystalline particles with reasonable magnetic properties will be demonstrated.

2. Experimental

2.1 *Synthesis*

Hexagonal Sr_2Y ferrite nanocrystalline powders with a chemical composition of $Sr_2Mg_2Fe_{12}O_{22}$ were prepared by the autocombustion method. The starting precursors were strontium nitrate ($Sr(NO_3)_2$, 99% purity), magnesium nitrate hexahydrate ($Mg(NO_3)_2{\cdot}6H_2O$, 98% purity), iron (III) nitrate nonahydrate ($Fe(NO_3)_3{\cdot}9H_2O$, 98–100% purity) (all from Alfa Aesar), and glycine ($C_2H_5NO_2$, 98.5% purity) (from Qualigens). All analytical reagents were used without any further purification. Initially, stoichiometric amounts of strontium nitrate ($Sr(NO_3)_2$), magnesium nitrate ($Mg(NO_3)_2{\cdot}6H_2O$) and ferric nitrate ($Fe(NO_3)_3{\cdot}9H_2O$) were dissolved in 20 ml of distilled water in a beaker, 10 ml of nitric acid (HNO_3) was introduced into the beaker to get a clear aqueous solution. The desired amount of glycine (fuel) was then added to the above solution, the whole mixture was stirred at a temperature of 100°C by a magnetic stirrer until the water slowly evaporated and the mixture became a dark brown viscous gel. This took about 2 h. The resulted dark brown viscous gel was kept on a hot plate at 200°C for about 10 min. By then the gel started to produce foams and sparks with the evolution of gaseous fumes. After the completion of combustion, a brownish powder was obtained. The time taken from actual ignition to the end of the reaction during the combustion process was less than 20 s. Finally, the as-prepared powder was grounded using an agate mortar and pestle to form a fine powder. A schematic diagram of the preparation step is given in figure 1.

2.2 *Characterization*

The crystal structure of the as-synthesized powders was identified by X-ray powder diffraction (XRD) measurements. XRD profiles were collected by Bruker D2 Phaser powder X-ray diffractometer with CuK_α radiation ($\lambda = 1.5418$ Å) over the range of 10° to 80° with a step mode of 0.02 min^{-1}. The as-synthesized powders were also analysed by FT–IR spectrophotometer (Bruker Alpha) using opus 6.5 (version) software. Small amounts of the as-synthesized powders were mixed with potassium bromide (KBr) and pressed into 1 mm thick transparent discs. IR spectra were collected from these discs. IR measurements were carried out at room temperature over the range 350–1400 cm^{-1}. Information about the oxidation states in

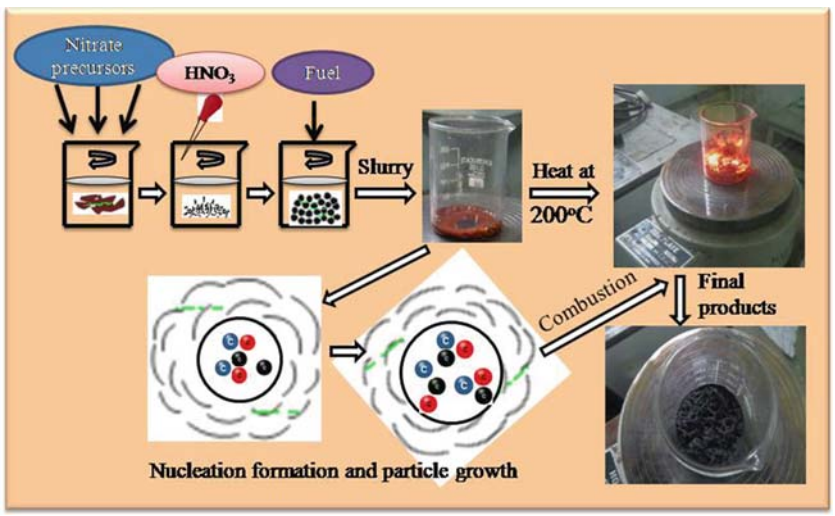

Figure 1. Schematic representation of Sr_2Y hexaferrite nanoparticles prepared by the combustion method.

the as-synthesized powders was obtained from X-ray photoelectron spectroscopy (XPS). XPS studies were performed by Kratos Analytical Axis Ultra DLD with Al Kα1 source. X-ray photon of 1.486 keV with a pass energy of 160 eV was used for the survey spectrum with 40 eV narrow scans. The spectra were collected using a combination of electrostatic and magnetic lens (hybrid mode) for an analysed area of 700 μm $\times$ 300 μm. Surface charging effects were minimized using a charge balance operating at 3.6 V and 1.8 V maintained as filament bias. The angle between the normal to the sample surface and the direction of photoelectron collection are perpendicular to each other. Casa XPS software was used for peak fitting, and the procedures and conditions of the analyses were kept consistent for all the samples. In brief, a Shirley background was used, and the relative area, full-width at half-maximum (FWHM), Lorentzian–Gaussian (20% L–80% G) ratios, and peak positions were allowed to vary. The number of peaks for fitting was manually varied, and the minimum number of peaks that gave a reasonable fit were used for the analysis. The surface morphology was analysed by Carl Zeiss ULTRA 55 field emission scanning electron microscope (FESEM). The samples were coated with a thin gold layer before FESEM imaging. This enabled a resolution of $\sim$1 nm at an acceleration voltage of 5 kV. The working distance was 1 mm. The magnetic measurements have been carried out using Lakeshore 7410 vibrating sample magnetometer (VSM) with applied magnetic fields up to 10 kOe at room temperature.

3. Results and discussion

3.1 *Gylcine-assisted combustion synthesis of $Sr_2Mg_2Fe_{12}O_{22}$*

The nanocrystalline Sr_2Y particles were synthesized by autocombustion; however, their physicochemical properties depend on the nature and the amount of the fuel used. In order to prepare pure nanocrystalline Sr_2Y particles, glycine was utilized as the suitable fuel. It is cost-effective and can be easily obtained compared to other organic fuels. The autocombustion method depends on fuels that act as the reducing agents and metal nitrates that act as oxidizing agents. The reducing valencies of strontium, magnesium, iron, carbon and hydrogen are +2, +2, +3, +4 and +1 respectively and the oxidizing valencies of oxygen and nitrogen are −2 and 0 respectively. The complete redox reaction of the metal nitrates with fuel (glycine) can be represented as

$$\begin{aligned} &Sr(NO_3)_2 + Mg(NO_3)_2 \\ &\quad + 5Fe(NO_3)_3{\cdot}9H_2O + 36.7NH_2CH_2COOH \\ &\longrightarrow SrFe_2O_4 + SrFe_{12}O_{19} + MgFe_2O_4 \\ &\quad + N_2 + CO_2 + H_2O \\ &\longrightarrow Sr_2Mg_2Fe_{12}O_{22}. \end{aligned} \quad (1)$$

In this reaction, the metal nitrates mix with carbon and hydrogen from the glycine fuel to form gaseous products like CO_2, N_2 and water molecule. The total calculated valences of metal nitrates were –220 and +9 for glycine (NH_2CH_2COOH). The stoichiometric composition of glycine–metal nitrates (Gly/NO^{3-}) mixture becomes $2\times(-10) + 2\times(-10) + 12\times(-15) + n(+9) = 0$, with $n = 24.44$ mol for this redox reaction. During the formation of Sr_2Y, the number of moles of gases produced per mole of oxide is about 24.44. The calculated amount of glycine will be 36.7 g (assuming 0.5 M).

The autocombustion is an explosive method which yields many grams of powder within a short period of time even though a small amount of the powder will be lost in the high flames during the combustion. Therefore, safety precautions have to be taken. In this work, we have chosen fuel–lean composition with Gly/NO^{3-} < 24.44 (glycine-to-nitrate ion molar ratio) which made the combustion reaction very mellow, and lose of powder in the high flames were greatly minimized. We estimated a loss of about 20% of the powder in the flames during the combustion process. For comparison, we used three different Gly/NO^{3-} molar ratios: 0.1818 (very fuel–lean reaction) and the powder produced is denoted as A-Sr_2Y, 0.712 (fuel–lean reaction) and the powder produced is denoted as B-Sr_2Y and 24.44 (fuel–stoichiometric reaction) and the powder produced is denoted as C-Sr_2Y.

3.2 *X-ray diffraction studies*

The X-ray diffraction (XRD) patterns of the prepared Sr_2Y nanocrystalline particles with different glycine-to-nitrate molar ratios are shown in figure 2. It can be seen that Gly/NO^{3-} ratio plays an important role in the formation and purity of the Sr_2Y nanocrystalline particles. For the A-Sr_2Y sample, a mixture of phases had formed. The fuel might not be enough to mix completely with the metals and the combustion process was incomplete. By increasing Gly/NO^{3-} ratio (fuel–lean reaction), i.e., B-Sr_2Y, a mixture of Sr_2Y hexaferrite and $Mg_2Fe_2O_4$ was formed. Upon

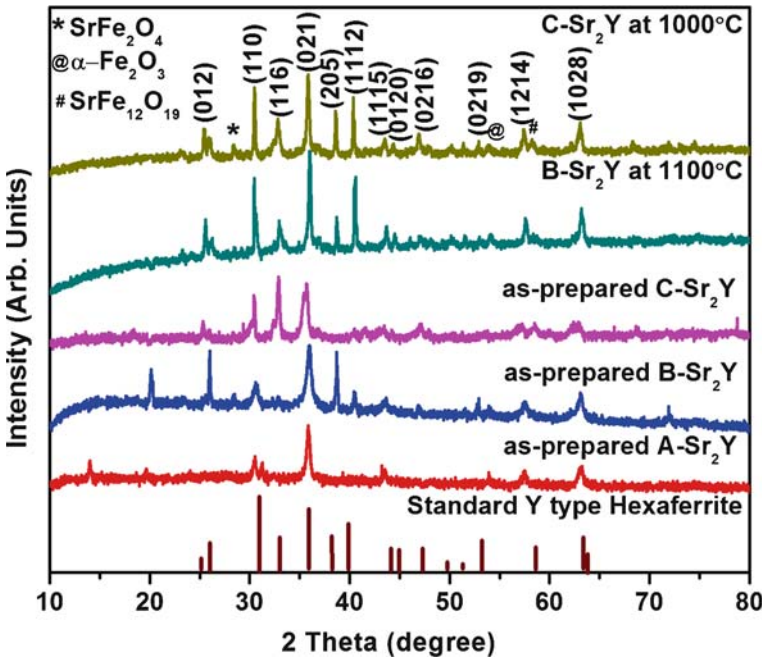

Figure 2. X-ray diffraction pattern of Sr_2Y hexaferrite nanoparticles prepared by the combustion method.

the calcination of the B-Sr_2Y powder at 1100°C, Sr_2Y hexaferrite phase became more pronounced. However, the obtained Sr_2Y hexaferrite nanocrystalline particles were not completely pure and contained minute quantities of impurities. The XRD peaks were matched with the standard ICDD data card (44-0206) for the Y-type hexaferrites. The as-synthesized C-Sr_2Y hexaferrite nanocrystalline particles (fuel-stoichiometric reaction) were much better than the B-Sr_2Y nanoparticles in terms of the formation of the Sr_2Y hexaferrite phase. However, XRD peaks around 36–40° are absent and this suggests that the sample needs to be calcined at higher temperatures to bring out the Y-type hexagonal phase. Upon calcination at 1000°C, we obtained a nearly pure phase of Sr_2Y hexaferrite with minute quantities of impurities such as $SrFe_2O_4$, αFe_2O_3 and $SrFe_{12}O_{19}$. Among the various stoichiometric compositions of glycine–metal nitrates mixture, the B-Sr_2Y calcined at 1100°C and the C-Sr_2Y calcined at 1000°C were found to be suitable for the formation of Sr_2Y hexaferrite nanocrystalline particles. The average crystallite size (t) of the prepared Sr_2Y hexaferrites was determined by the X-ray line broadening method in accordance with the Scherrer equation [5]

$$t = 0.9\lambda/(\beta \cos\theta), \tag{2}$$

where λ (0.154 nm) is the wavelength of X-ray, β is the full-width at half-maximum (FWHM) and θ is the Bragg's diffraction angle. This equation does not include any effects of the strains. The breadth of diffraction peaks in the XRD pattern were corrected for instrumentation broadening. The average crystallite size was found to be 45 nm for the 1100°C calcined B-Sr_2Y hexaferrites and 53 nm for the 1000°C calcined C-Sr_2Y hexaferrites. These values are comparable with the values of 56 nm (conventional sol–gel) and 34 nm (microwave heating) found for Y-type $Ba_2Co_2Fe_{12}O_{22}$ [6].

The lattice constants for Sr_2Y hexaferrites were calculated from the following equation [7]:

$$1/d_{hkl} = [4/3(h^2 + hk + k^2/a) + l^2/c^2]^{1/2}, \tag{3}$$

where d is the value of d-spacing of the line in XRD pattern and (hkl) are the Miller indices. The calculated values of lattice parameters of the B-Sr_2Y hexaferrites nanocrystalline particles calcined at 1100°C were $a = 5.89$ Å and $c = 43.610$ Å with an accuracy of ±0.002 Å, whereas for the C-Sr_2Y hexaferrites calcined at 1000°C, $a = 5.97$ Å and $c = 43.703$ Å. These values are in good agreement with that of $Ba_2Ni_2Fe_{12}O_{22}$ ($a = 5.859$ Å, $c = 43.504$ Å) and $Ba_2Co_2Fe_{12}O_{22}$ ($a = 5.86$ Å, $c = 43.504$ Å) in accordance with JCPDS Card No. 44-0206 [7].

The volumes of unit cells (V_{cell}) of the calcined Sr_2Y hexaferrites were determined using the following equation [7]:

$$V_{cell} = a^2 c \sin 120°. \quad (4)$$

The calculated value of unit cell volume for the B-Sr_2Y hexaferrites calcined at 1100°C was 1325.134 Å^3 and for the C-Sr_2Y hexaferrites calcined at 1000°C was 1310.546 Å^3 (±0.0002).

The X-ray density d_X of the calcined Sr_2Y hexaferrites were calculated using the following expression [8]:

$$d_X = ZM/N_A V_{cell}, \quad (5)$$

where Z is the number of molecules per unit cell, M is the molecular weight of the sample, N_A is the Avogadro's number = 6.023×10^{23} and V_{cell} is the unit cell volume. The values of X-ray density were found to be 6.273 g cm^{-3} and 6.201 g cm^{-3} for the calcined B-Sr_2Y and C-Sr_2Y hexaferrite respectively. These values are comparable with the values of 5.138 g cm^{-3} for $Sr_2Co_2Fe_{12}O_{22}$ and 5.44 g cm^{-3} for $Ba_2Ni_2Fe_{12}O_{22}$ [7,9].

The specific surface area (S) of the calcined Sr_2Y hexaferrite nanocrystalline particles was calculated from the X-ray density (d_X) and the average crystallite size (t) in accordance with the following equation [10]:

$$S = 6/d_X D. \quad (6)$$

The specific surface area was found to be 18.046 m^2 g^{-1} for the calcined B-Sr_2Y and 21.459 m^2 g^{-1} for calcined C-Sr_2Y hexaferrite nanoparticles.

3.3 *FTIR analysis*

Fourier transform infrared (FTIR) spectroscopy was used to gather information on the ions within the structure of calcined Sr_2Y hexaferrites. The FTIR spectra of the calcined B-Sr_2Y and C-Sr_2Y hexaferrites are shown in figure 3. The vibrational characteristics of one group of atoms within the network of different sublattices are usually independent of the vibrations of the other groups. This can provide significant information on the arrangement of atoms in hexaferrite particles. The characteristic IR absorption bands for the calcined B-Sr_2Y are assigned as follows: the absorption band at 3426.8 cm^{-1} is attributed to the fundamental vibrational modes of the OH group and the two weak IR bands at 2921.8 cm^{-1} and 2857 cm^{-1} originate from the C–H stretching vibrations. The IR absorption bands at 1746.5 cm^{-1} and 1635.6 cm^{-1} can be attributed to the asymmetrical and symmetrical stretching vibrations of the CO^{2-} group. The IR band at 1454 cm^{-1} can be attributed to the N–O stretching vibrations of NO^{3-} (nitrate) group. The band at 856.6 cm^{-1} can be attributed to the vibrational frequency of the octahedral sites in the S and T blocks of the whole complex Y-type

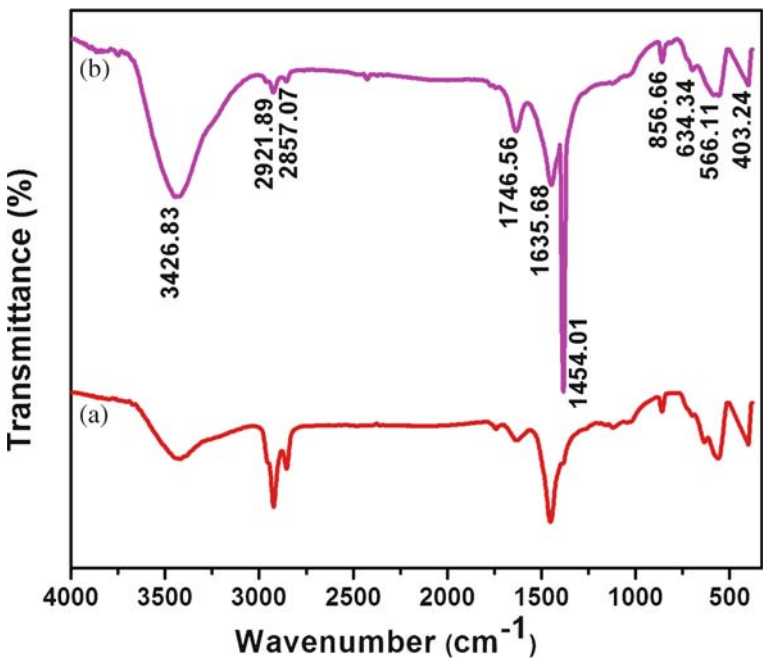

Figure 3. FTIR spectrum of (**a**) B-Sr_2Y hexaferrite nanoparticles at 1100°C and (**b**) C-Sr_2Y hexaferrite nanoparticles at 1000°C prepared by the combustion method.

structure. The IR band at 634.3 cm^{-1} is attributed to the octahedral sites in T–S block boundaries. The absorption band at about 566.1 cm^{-1} is attributed to the octahedral group in spinel blocks. The band at 403.24 cm^{-1} is attributed to the Fe–O stretching vibrations of the tetrahedral complexes in spinel blocks. Similar results were also observed for the calcined C-Sr_2Y hexaferrite with small variations over the same range. These observations confirmed the chemical structure and positions of the ions within the prepared Sr_2Y heaxaferrite nanocrystalline particles. The IR results are consistent with crystal structure observed from the XRD measurements. The calcined Sr_2Y hexaferrites have nearly single phase with minute impurity phases.

3.4 *X-ray photoelectron spectroscopy studies*

X-ray photoelectron spectroscopy (XPS) studies were performed to determine the chemical species and states of the elements in our samples. Figure 4a shows the wide spectrum of calcined C-Sr_2Y hexaferrites nanocrystalline particles. The elements such as Sr, Mg, Fe, C and O were detected. No other elements were identified; this supports the nearly single phase obtained from the XRD analyses.

Figure 4c shows the Sr 3*d* XPS deconvolution spectra for the calcined nanocrystalline C-Sr_2Y hexaferrites. The Sr 3*d* peak is split into two peaks, namely Sr $3d_{5/2}$ and Sr $3d_{3/2}$, due to the spin orbital coupling. The Sr $3d_{5/2}$ can be resolved into two consecutive peaks with binding energies of 131.9 eV and 132.6 eV which are assigned to Sr^{1+} and Sr^{2+} ions. The Sr $3d_{3/2}$ can be resolved into two peaks at 133.6 eV and 134.8 eV corresponding to the binding energies of Sr^{1+} and Sr^{2+} ions. The difference of about 1.2 eV between the two peaks of Sr $3d_{3/2}$ is attributed to Sr^{2+} ion as reported in previous studies [11]. Figure 4d shows the Sr 3*p* XPS spectra for the C-Sr_2Y hexaferrites calcined at 1000°C. The Sr 3*p* contains a C 1*s* peak. This may have resulted from minute quantities of impurities left in the sample from the combustion process. Based on spin-orbital splitting, the Sr 3*p* splits into two doublet peaks such as Sr $3p_{3/2}$ and Sr $3p_{1/2}$. This doublet peaks are well deconvoluted with binding energy splitting of 10.3 eV corresponding to the Sr^{2+} ion in its oxide environment [12,13].

Figure 4b shows the deconvolution of Mg 2*p* spectra for the calcined nanocrystalline C-Sr_2Y hexaferrites. These spectra are fitted with the raw data and deconvoluted to resolve the peaks. The Mg 2*p* core level is close to the valence band and the difference between

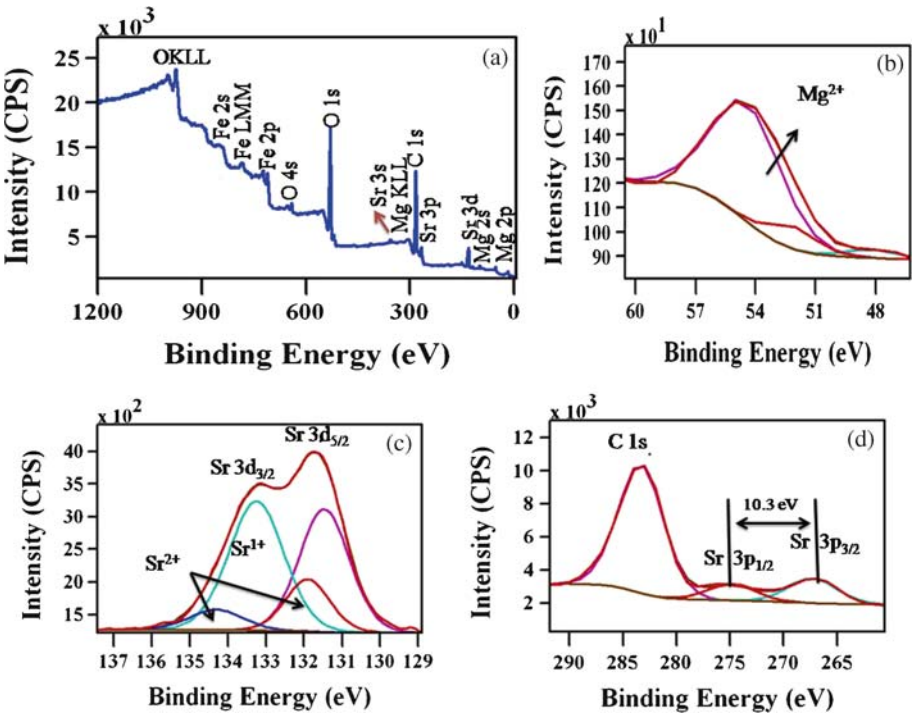

Figure 4. (**a**) XPS survey spectrum, (**b**) deconvolution spectra of Mg 2*p* peak, (**c**, **d**) high-resolution spectra of Sr 3*d* and Sr 3*p* peaks for C-Sr_2Y hexaferrite nanoparticles at 1000°C.

Mg $2p_{3/2}$ and Mg $2p_{1/2}$ cannot be resolved. This is expected to reveal the charge and valence state of Mg more representatively. Gaussian fit was applied to the Mg $2p$ peak and it was resolved into three distinct components. The minor peak at the lower binding energy of 49.5 eV is attributed to the metallic Mg which is good agreement with previous reports [14,15]. The peak at 51.6 eV is assigned to MgB_2 [15]. The major peak at the higher binding energy of 54.4 eV is attributed to the divalent (Mg^{2+}) species of Mg [15].

The Fe $2p$ photoelectron peak of the calcined nanocrystalline C-Sr_2Y hexaferrite particles is shown in figure 5a. Based on spin-orbit coupling, the Fe $2p$ peak is split into Fe $2p_{3/2}$ and Fe $2p_{1/2}$ components. The Fe $2p_{3/2}$ peak can be deconvoluted into two peaks at 709.14 eV and 710.60 eV corresponding to the binding energies of Fe^{2+} and Fe^{3+} ions. Similarly, Fe $2p_{1/2}$ peak can be deconvoluted into two fine peaks at 723.02 eV and 725.78 eV attributed to Fe^{2+} and Fe^{3+} ions. However, a peak at 717.80 eV is present between the Fe $2p_{3/2}$ and Fe $2p_{1/2}$ components and it is considered as satellite peak. Due to large background, the chemical states of Fe are difficult to analyse. The difference of about 8.66 eV between the binding energies of the satellite peak and the principal peak of Fe $2p_{3/2}$ is due to the presence of Fe^{3+} ion

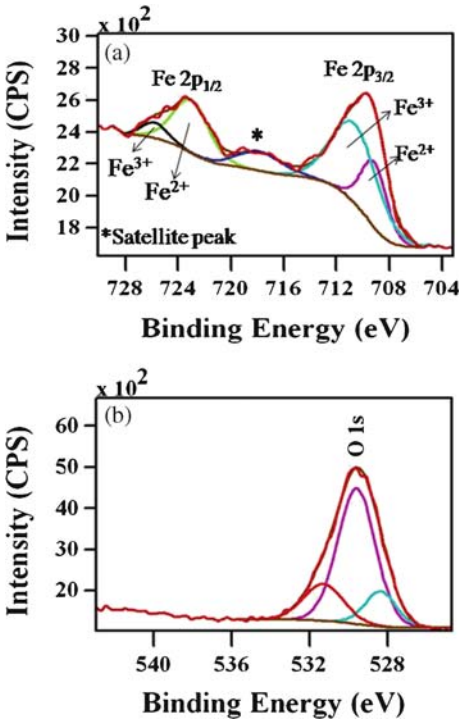

Figure 5. (**a**) High-resolution spectra of Fe $2p$ peak and (**b**) XPS spectra for O $1s$ peak for C-Sr_2Y hexaferrite nanoparticles at 1000°C.

[16–18]. In principle, the valence of Fe ions fluctuate due to the reduction of Fe^{3+} to Fe^{2+} ions. In order to determine the presence of oxide/hydroxide species in the prepared samples, O $1s$ spectra were analysed. Figure 5b shows the deconvolution of the spectra for the calcined C-Sr_2Y hexaferrites. The O $1s$ peak can be decomposed into three peaks. The first peak at 528.51 eV is attributed to lattice O^{2-}, the second peak at 529.72 eV is assigned to the lattice OH^- contribution from $Fe(OH)_2$ and FeOOH and the third peak at 531.33 eV corresponds to the adsorbed –H–O–H on the surface of the Sr_2Y hexaferrites [19].

3.5 *Morphology studies*

The morphology of the prepared nanocrystalline hexaferrite particles were examined by FESEM. The FESEM images of the calcined C-Sr_2Y hexaferrite nanoparticles at different magnifications are shown in figure 6. The Sr_2Y hexaferrites have dense microstructure with uniform particle size distribution. Almost all the particles have hexagonal symmetry with definite crystalline grain boundaries. The shape of the grains in the hexaferrites determines the right technological application. Rod-shaped hexaferrites can be utilized in surface-enhanced Raman scattering, imaging, catalysis, data storage and sensing [20,21]. Platelet-shaped hexaferrites may be suitable as microwave absorption coating [29]. In the present study, the grains grew larger and became compactly stacked as the sintering temperature was raised. Obviously, the porosity and grain boundaries decrease with the rise of the sintering temperature [22]. The prepared nanocrystalline Sr_2Y hexaferrite particles with larger grain size might be suitable as microwave absorbing materials.

3.6 *Magnetic studies*

The magnetization of the present calcined Sr_2Y hexaferrites was measured using vibrating sample magnetometer. Figure 7 shows plots of the individual hysteresis loops of the calcined B-Sr_2Y and C-Sr_2Y hexaferrites with applied magnetic fields up to 10 kOe. From these hysteresis loops, we can see that the saturation magnetization (M_s) was high, while the coercivity (H_c) was low. The values of saturation magnetization (M_s), coercivity (H_c) and remanence magnetization (M_r) obtained from the hysteresis loops are listed in table 1. From the observed values of the coercivity (H_c), it is clear that the calcined B-Sr_2Y and C-Sr_2Y show soft magnetic behaviour. It has been reported

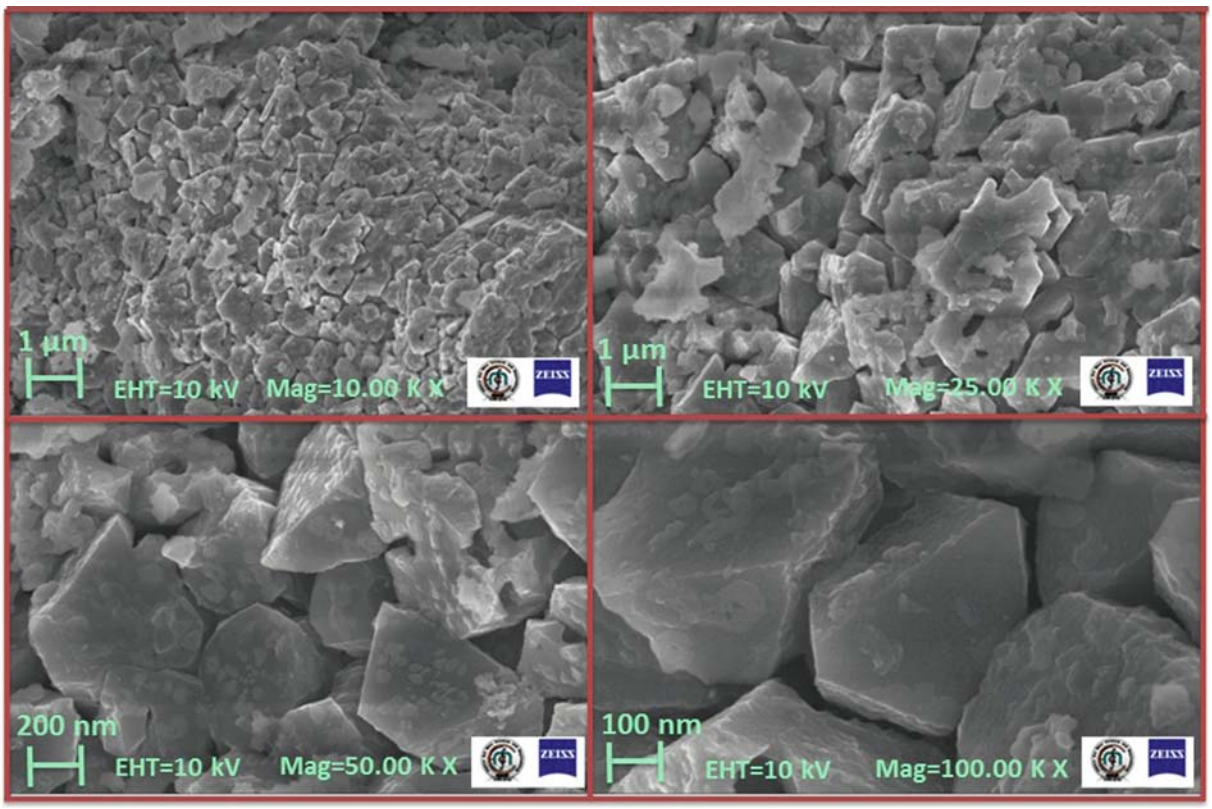

Figure 6. FESEM images of C-Sr_2Y hexaferrite nanoparticles at 1000°C with different magnifications.

earlier that the observed soft magnetic behaviour in ferrites is very significant for various practical applications in the fields of sensing, switching and security [23,24].

The room-temperature saturation magnetization (M_s) of the calcined B-Sr_2Y and C-Sr_2Y nanocrystalline hexaferrite particles was found to be 42.44 and 38.72 emu g^{-1} respectively. Similar results have been

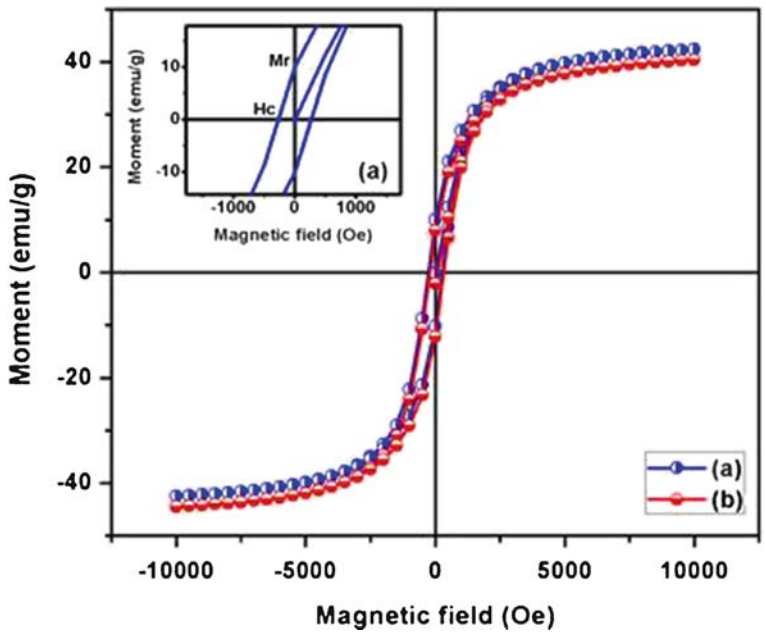

Figure 7. *M–H* loop of (**a**) B-Sr_2Y hexaferrite nanoparticles at 1100°C and (**b**) C-Sr_2Y hexaferrite nanoparticles at 1000°C with applied magnetic field up to 10 kOe. Inset figure shows the magnified view of B-Sr_2Y at 1100°C.

Table 1. Magnetic parameters obtained from synthesized Sr_2Y hexaferrite nanoparticles in comparsion with other Y-type hexaferrites.

Y-type hexaferrites	Synthesis	H_c (kA m^{-1})	M_s (emu g^{-1})	M_r (emu g^{-1})	SQR	Ref.
Ni_2Y	Gel to crystallite conversion method at 950°C	16	25.5	–	–	[24]
Mg_2Y	–	–	23	–	–	[25]
Zn_2Y	–	–	42	–	–	[25]
Mn_2Y	–	–	31	–	–	[25]
$Zn_{1.2}Cu_{0.8}Y$	1050°C	6.8	34.5	4.05	–	[27]
Co_2Y	–	4.4	34	–	–	[25,29]
	Sol–gel derived fibres, 1000°C	30	32.8	–	–	[30]
	EDTA complex synthesis	15–6.7	28.8–33.4	5.3–14.4	–	[31]
	1000°C	12.7	26.6	–	–	[32,33]
Sr_2Y	Combustion method at 1100°C	21.33	42.44	10.05	0.24	This work
	1000°C	19.66	38.72	13.19	0.34	

reported for various Y-type hexaferrites [25–27]. Generally, differences in M_s depend on the temperature of calcination and particle size [28]. In our work, it is observed that the saturation magnetization slightly decreased by varying the fuel stoichiometric ratio conditions and the calcining temperature. The values of coercivity (H_c) of the calcined B-Sr_2Y and C-Sr_2Y hexaferrites were found to be 21.33 and 19.66 kA m^{-1} which are in good agreement with various values for Y-type hexaferrites reported by other groups [29–33]. The values of remanence magnetization or retentivity (M_r) extracted from the M–H loop were found to be 10.05, 13.19 emu g^{-1} for the calcined B-Sr_2Y and C-Sr_2Y nanocrystalline hexaferrite particles. The squareness ratios (SQR) were calculated from the values of M_s and M_r and found to be 0.24 and 0.34 for the calcined B-Sr_2Y and C-Sr_2Y hexaferrites respectively. In general, large SQR values are preferred for many applications such as magnetic recording media and permanent magnets. The magnetic parameters of the prepared Sr_2Y samples in this study are not only correlated with the grain size but also with the preparation conditions. It is possible to obtain higher quality samples with desirable magnetic properties by optimizing the processing parameters of the preparation.

4. Conclusion

A new compound of Sr-based Y-type hexaferrite was successfully synthesized by autocombustion using glycine as the fuel. The newly prepared nanocrystalline Sr_2Y hexaferrite particles were characterized by XRD, FESEM, FTIR, XPS and VSM. The formation of a single phase with a nominal chemical composition of $Sr_2Mg_2Fe_{12}O_{22}$ hexaferrites was demonstrated. The prepared Sr_2Y hexaferrites showed good magnetic properties similar to that of the Y-type hexaferrites. The preparation of nanocrystalline Sr_2Y hexaferrites particles depends on the initial conditions of the autocombustion and calcination treatments.

References

[1] H R Kirchmayr, *J. Phys. D* **29**, 2763 (1996)
[2] D Lisjak and M Drofenik, *J. Eur. Ceram. Soc.* **24**, 1841 (2004)
[3] F Leceabue, R Painzzieri, G Albanese, G Leo and N Suarez, *Mater. Res. Bull.* **33**, 266 (1988)
[4] K Haneda and H Kojima, *J. Phys. Status Solidi A* **6**, 259 (1971)
[5] R Tholkappiyan and K Vishista, *Adv. Sci., Eng. Med.* **6**, 311 (2014)
[6] M Barkat Ul-ain, Safeer Ahmed, Yanqiang Huang, Aiqin Wang and Tao Zhang, *J. Mater. Chem.* **22**, 22190 (2012)
[7] Mukhtar Ahmad, Qasim Ali, Ihsan Ali, Ishtiaq Ahmad, M Azhar Khan, Majid Niaz Akhtar, G Murtaza and M U Rana, *J. Alloys Compounds* **580**, 23 (2013)
[8] V Vaishali Soman, V M Nanoti and D K Kulkarni, *Mat. Manufacturing Proc.* **29**, 397 (2014)
[9] Ihsan Ali, Mukhtar Ahmad, M U Islam and M S Awan, *J. Sol-Gel Sci. Technol.* **68**, 141 (2013)
[10] M George, A M John, S S Nair, P A Joy and M R Anantharaman, *J. Magn. Magn. Mater.* **302**, 190 (2006)
[11] M P De Jong, V A Dediu, C Taliani and W R Salaneck, *J. Appl. Phys.* **94**, 7292 (2003)
[12] V V Atuchin, J C Grivel, A S Korotkov and Z Zhang, *J. Solid State Chem.* **181**, 1285 (2008)
[13] V V Atuchin, J C Grivel and Z Zhang, *Chem. Phys.* **360**, 74 (2009)
[14] R P Vasquez, C U Jung, Min-Seok Park, Hoon-Jung Kim, J Y Kim and Sung-Ik Lee, *Phys. Rev. B* **64**, 052510 (2001)

[15] K B Garg, T Chatterji, S Dalela, M Heinonnen, J Leiro, B Dalela and R K Singhal, *Solid State Commun.* **131**, 343 (2004)
[16] Liu Liangjun, Guoliang Zhang, Ling Wang, Tao Huang and Lei Qin, *Ind. Eng. Chem. Res.* **50**, 7219 (2011)
[17] Akihiko Miyakoshi, Akifumi Ueno and Masaru Ichikawa, *J. Appl. Catal. A* **219**, 249 (2001)
[18] F Tihay, G Pourroy, Richard-Plouet, M Roger and A C Kiennemann, *J. Appl. Catal. A* **206**, 29 (2001)
[19] R Tholkappiyan and K Vishista, *Solar Energy* **106**, 118 (2014)
[20] D Srivastava and I Lee, *Adv. Mater.* **18**, 2471 (2006)
[21] H Wang, D W Brandle, F Le, P Nordlander and N Halas, *J. Nano Lett.* **6**, 827 (2006)
[22] Baia Yang, Xu Fang, Qiao Lijie and Zhou Ji, *J. Alloys Compounds* **473**, 505 (2009)
[23] Mukhtar Ahmad, R Grossinger, M Kriegisch, F Kubel and M U Rana, *Curr. Appl. Phys.* **12**, 1413 (2012)
[24] Mukhtar Ahmad, R Grossinger, M Kriegisch, F Kubel and M U Rana, *J. Magn. Magn. Mater.* **332**, 137 (2013)
[25] J Smit and H P J Wijn, *Ferrites* (Philips Technical Library, Eindhoven, 1959)
[26] C Sudakar, G N Subbanna and T R N Kutty, *J. Magn. Magn. Mater.* **263**, 253 (2003)
[27] Y Bai, J Zhou, Z Gui and L Li, *Mater. Lett.* **58**, 1602 (2004)
[28] B Aslibeiki, P Kameli, H Salamati, M Eshraghi and T Tahmasebi, *J. Magn. Magn. Mater.* **322(19)**, 2929 (2010)
[29] M Obol and C Vittoria, *IEEE Trans. Magn.* **39**, 3103 (2003)
[30] R C Pullar, I K Bdikin and A K Bhattacharya, *J. Euro. Ceram. Soc.* **32**, 905 (2012)
[31] C Zhang, J Shi, X Yang, L De and X Wang, *Mater. Chem. Phys.* **123**, 551 (2010)
[32] Y Bai, J Zhou, Z Gui, Z Yue and L Li, *J. Magn. Magn. Mater.* **264**, 44 (2003)
[33] S G Lee and S J Kwon, *J. Magn. Magn. Mater.* **153**, 279 (1996)